Global and Regional Variations in Transthyretin Cardiac Amyloidosis: A Comparison of Longitudinal Strain and ^{99m}Tc-Pyrophosphate Imaging

Christopher Lee*[1], Chieh-Ju Chao*[1], Pradyumna Agasthi[1], Amith R. Seri[1], Amar Shere[1], Lanyu Mi[2], Lisa Brown[1], Chance Marostica[1], Timothy Barry[1], Ming Yang[3], Julie Rosenthal[1], Samuel Unzek[4], Farouk Mookadam[1], and Reza Arsanjani[1]

[1]*Department of Cardiovascular Diseases, Mayo Clinic Arizona, Phoenix, Arizona;* [2]*Department of Research, Division of Biomedical Statistics and Informatics, Mayo Clinic Arizona, Phoenix, Arizona;* [3]*Department of Radiology, Mayo Clinic Arizona, Phoenix, Arizona; and* [4]*Banner–University Medical Center Phoenix, Phoenix, Arizona*

There are limited data on the head-to-head comparison of ^{99m}Tc-pyrophosphate (^{99m}Tc-PYP) and echocardiographic strain imaging in the assessment of transthyretin (TTR) cardiac amyloidosis. **Methods:** At Mayo Clinic Arizona, patients who had undergone both a ^{99m}Tc-PYP scan and a transthoracic echocardiogram within a 90-d period were retrospectively identified for chart review and strain imaging analysis. Patients were divided into 2 groups according to their ^{99m}Tc-PYP results (PYP-positive [PYP+] or PYP-negative [PYP−]) for the comparison. A standard 17-segment model was used for segmental, regional, and global longitudinal strain comparison. A P value of less than 0.05 was deemed significant. **Results:** In total, 64 patients were included, the mean age was 75.1 ± 13.0 y, and 57 (89.1%) were male. Comparing the PYP+ to the PYP− group, the left ventricular global longitudinal strain was significantly worse in the former (PYP+ vs. PYP−, −10.5 ± 2.6 vs. −13.1 ± 4.1; $P = 0.003$). PYP+ patients also had worse regional basal strain (−4.6 ± 2.6 vs. −8.8 ± 4.0, $P < 0.001$) and a trend toward worse midventricular strain (−9.6 ± 4.0 vs. −11.7 ± 4.4, $P = 0.07$), but there was no statistical difference in the apical region (−17.6 ± 4.73 vs. −19.0 ± 6.46, $P = 0.35$). This is consistent with an apex-sparing pattern shown by the relative apical longitudinal strain index (1.3 ± 0.5 vs. 1.0 ± 0.3, $P = 0.008$). Segment-to-segment analysis demonstrated a significant difference in strain between PYP+ and PYP− segments in 4 segments: basal inferior ($P = 0.006$), basal anterolateral ($P = 0.01$), apical septal ($P = 0.002$), and apical inferior ($P = 0.001$). Left ventricular diastolic dysfunction was significantly different, with 17 (77.3%) patients in the PYP+ group versus 15 (36.6%) in PYP− participants ($P = 0.002$). **Conclusion:** Our study suggested that ^{99m}Tc-PYP uptake is related to overall worse LV segmental, regional, and global longitudinal strain function, as well as diastolic function, compared with patients without ^{99m}Tc-PYP uptake. These data are important for helping clinicians learn about the echocardiographic function features related to ^{99m}Tc-PYP uptake and can help generate hypotheses for future studies.

Key Words: cardiology; correlative imaging; ^{99m}Tc-pyrophosphate imaging; longitudinal strain; transthyretin cardiac amyloidosis

Received Jan. 3, 2021; revision accepted Aug. 5, 2021.

For correspondence or reprints, contact Christopher Lee (christopherlee@penmedicine.edu).

*Contributed equally to this work.

Published online Dec. 21, 2021.

J Nucl Med Technol 2022; 50:30–37
DOI: 10.2967/jnmt.120.261893

Amyloidosis is a heterogeneous group of disorders involving the extracellular deposition of insoluble amyloid protein that can occur in different organs. Amyloidosis can be either inherited or acquired. The cardiac manifestation of amyloidosis includes heart failure, conduction disease, syncope, and sudden cardiac death (*1*). So far, whereas over 30 different amyloidogenic proteins have been described, cardiac amyloid deposition and the development of cardiomyopathy are associated with types of amyloid proteins, most commonly transthyretin (TTR) and amyloid light chain (AL) proteins (*2*).

Concerning the diagnosis of cardiac amyloidosis (CA), endomyocardial biopsy–demonstrated amyloid deposition remains the gold standard and is also important for protein typing (*3*). However, newer noninvasive approaches can potentially allow earlier detection of CA with a minimal side-effect profile. In patients with a noncardiac biopsy demonstrating amyloid deposition, cardiac involvement has been defined—by a consensus opinion from the 10th International Symposium on Amyloidosis—as either a positive heart biopsy and or increased left ventricular (LV) wall thickness (interventricular septal thickness > 12 mm) in the absence of hypertension or other potential causes of true LV hypertrophy (*4*). Making an early diagnosis of cardiac amyloid has significant clinical implications concerning the poor prognosis of late-stage CA (*1,5*). However, as of 2019, TTR remained underdiagnosed; there were still 10%–15% of older adults with heart failure who might have unrecognized wild-type TTR (*5*).

Historically, the diagnosis of CA had involved a high index of clinical suspicion and consideration of a constellation of symptoms. Increased wall thickness noted on the echocardiogram was initially seen as a clue to CA; however, the same finding can also be present in other clinical conditions, such

as hypertrophic cardiomyopathy and hypertensive heart disease (*6,7*). In clinical practice, a comprehensive evaluation of echocardiography parameters or involving other noninvasive studies is generally required to better differentiate these conditions. The characteristic apex-sparing pattern of myocardial strain distribution was suggestive of CA rather than other etiologies when the initial echocardiographic findings raised the concerns (*7–9*). The apex-sparing strain pattern has been observed in both AL- and TTR-type CA (*10,11*). A difference in myocardial strain dysfunction between different subtypes has also been reported (*10*).

The other widely used noninvasive modality is ^{99m}Tc-pyrophosphate (^{99m}Tc-PYP) imaging, which is highly sensitive and specific for the diagnosis of TTR-related amyloidosis without the need for endomyocardial biopsy (*12*). A recent European study using ^{99m}Tc-hydroxymethylene diphosphonate determined the regional distribution of nuclear tracer uptake in patients with TTR-related CM, a distribution that was similar to the apex-sparing pattern of strain echocardiographic imaging (*13*). The difference in uptake by human TTR and AL cardiac tissues is believed to be related to the microcalcifications in human TTR cardiac tissue, which are more common than in AL cardiac tissue (*14*).

Despite being commonly used for the assessment of CA, strain echocardiography and ^{99m}Tc-PYP imaging findings have yet to be compared directly with each other. Differences in echocardiographic parameters were also reported between the AL and TTR subtypes of CA.

We designed this study to compare the echocardiographic strain distribution patterns between patients with positive ^{99m}Tc-PYP results (PYP+ group) and negative ^{99m}Tc-PYP results (PYP− group). We hypothesized that ^{99m}Tc-PYP uptake correlates with worse echocardiographic LV strain function.

MATERIALS AND METHODS

The study protocol complied with the Declaration of Helsinki and was approved by the Mayo Clinic institutional review board. Informed consent was waived because the study was deemed to pose minimal risk (retrospective chart review and data analysis only).

Patient Population

All consecutive patients who had undergone both ^{99m}Tc-PYP scanning for suspected CA and, within 90 d, transthoracic echocardiography from October 2015 to March 2018 at a single center (Mayo Clinic, Arizona) were retrospectively selected. There was a high clinical suspicion of CA in these individuals, including increased LV wall thickness in the absence of significant hypertension, and findings were more suggestive of CA than of hypertrophic cardiomyopathy. These individuals subsequently underwent serum protein electrophoresis, urine protein electrophoresis, and a serum free light chain assay and were then referred for ^{99m}Tc-PYP scanning (*15*).

Each patient's transthoracic echocardiogram study was reviewed for image-quality selection criteria, which included acceptable-quality echocardiogram images of the standard apical 4-, 3-, and 2-chamber views, to allow for complete strain imaging analysis. Adequate quality was defined as no more than 2 segments of unreadable strain, which was the only metric that resulted in exclusion of otherwise eligible participants from final analysis.

Patient Demographics, Electrocardiograms, Biomarkers, and Ancillary Data

Detailed review of electronic health records yielded a broad dataset, including participant demographics (age, sex), body mass index (kg/m^2), creatinine, estimated glomerular filtration rates, troponin, N-terminal prohormone B-type natriuretic protein, and clinical parameters such as the presence or absence of low voltage on electrocardiography, pleural effusion, and pericardial effusion.

Echocardiography and Strain Imaging

Measurement of LV diastolic function, including descriptions and acquisition of specific parameters, has been outlined by Nagueh et al. (*16*). The original transthoracic echocardiogram reports were reviewed to obtain echocardiographic structural, systolic, and diastolic functional parameters, including LV ejection fraction (%), LV mass (g), LV mass index (g/m^2), LV stroke volume (mL), cardiac index (L/m^2/min), mitral E-wave velocity (m/s), mitral A-wave velocity (m/s), mitral E/A ratio, mitral E wave deceleration time (ms), tissue Doppler medial e′ velocity (m/s), E/e′ ratio medial, E/e′ ratio lateral, tricuspid annulus systolic excursion by M-mode (mm), right ventricular systolic pressure (mm Hg), and the presence of diastolic dysfunction. All echocardiographic parameters were measured according to the American Society of Echocardiography guidelines (*17,18*).

Strain imaging was retrospectively completed using commercial software, EchoInsight (Trust Bio-sonics). Strain imaging was initially generated using the 18-segment model. Global longitudinal strain (GLS) and regional longitudinal strain values for the apical, mid, and basal regions were abstracted as reported by EchoInsight. Both strain and ^{99m}Tc-PYP imaging were represented using the standard 17-segment American Heart Association model (*18*). Strain modeling was converted from the 18-segment model to the 17-segment model to allow direct comparability (Fig. 1). This conversion process involved averaging of strain segments 13–18 from the 18-segment model; this average was then taken to represent segments 13–17 in the 17-segment model.

^{99m}Tc-PYP Imaging

^{99m}Tc-PYP scanning was performed using a standard American Society of Nuclear Cardiology protocol containing both planar and SPECT/CT series (*18*). After intravenous administration of 370 MBq of ^{99m}T-PYP, 15-min and 3-h delayed anterior-view planar images of the chest (matrix, 256 × 256) were acquired, followed by a SPECT/CT scan of the chest.

On the 3-h anterior planar image, circular regions of interest were placed around the heart and contralateral right chest to measure the counts and calculate the heart–to–contralateral-lung ratio (heart-to-contralateral ratio). Heart-to-contralateral values higher than 1.4 are considered indicative of TTR CA with a high PPV. Heart-to-contralateral values in the range of 1.3–1.4 can be seen with TTR amyloidosis, especially when activity is seen in the myocardium on SPECT/CT.

On SPECT/CT images, semiquantitative grading (0–3 scale) is based on visual inspection of tracer uptake in the myocardium, compared with that in the rib (*19*).

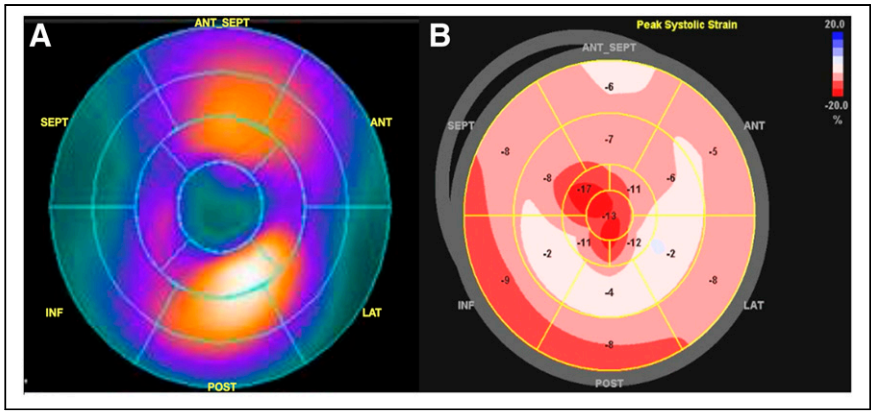

FIGURE 1. Side-by-side comparison of American Heart Association 17-segment model bull's-eye color-mapping plots of ^{99m}Tc-PYP scan (A) and speckle-tracking strain imaging (B) in representative case with positive ^{99m}Tc-PYP findings. Panel A demonstrates intense LV myocardium uptake in anterior and inferior segments and no uptake at apex. Panel B demonstrates characteristic apex-sparing distribution pattern of peak LV longitudinal systolic strain. In this case, segments with uptake are associated with worse strain function. Values in panel B stand for segmental peak longitudinal systolic strain of each segment. ANT = anterior; INF = inferior; LAT = lateral; POST = posterior; SEPT = septal.

Other variables include the heart-to-contralateral ratio of the counts on anterior view planar scintigraphy images and a SPECT/CT-based semiquantitative scale of the myocardial radiotracer uptake. A positive ^{99m}Tc-PYP scan is defined as one on which any of the 17 segments is deemed to be ^{99m}Tc-PYP–positive according to the American Society of Nuclear Cardiology guidelines (*20*). ^{99m}Tc-PYP scan results were reported using the bull's-eye 17-segment model.

Electrocardiograms, Biomarkers, and Ancillary Data

The electronic health records were reviewed for patient demographic and other clinical data, including participant demographics (age, sex), body mass index, serum creatinine, estimated glomerular filtration rates, troponin, N-terminal prohormone B-type natriuretic protein, and clinical parameters such as the presence or absence of low voltage on electrocardiography, pleural effusion, and pericardial effusion.

Statistical Analysis

Descriptive statistics are used to summarize demographic and clinical characteristics. Mean and SD, with 2-sample *t* testing for group comparison, are presented for normally distributed continuous variables, and median and interquartile range, with Wilcoxon rank-sum testing, are used to describe nonnormally distributed continuous data. Categoric variables are summarized as frequency (%), with Fisher exact testing for comparison. As for strain imaging parameters, a 2-sample *t* test was used for global, regional, and segmental analysis. The 17 segments were categorized into 3 regions (basal, mid, and apical) for regional analysis. Relative apical longitudinal strain index (RALSI) was calculated as average apical LS/average basal LS + average mid LS (*8*). Regional analysis was done to compare the mean longitudinal strain between participants with positive ^{99m}Tc-PYP findings in any segment and those with a completely negative ^{99m}Tc-PYP scan. Segment analysis was done to compare the mean strain in PYP+ versus PYP− participants in each corresponding segment. The analysis was conducted using SAS 9.4 (SAS Institute). All tests were 2-sided, and a P value of less than 0.05 was considered statistically significant.

Pearson correlation between ^{99m}Tc-PYP scan findings and strain parameters, with graphical illustration, is shown in Supplemental Tables 1–4 (supplemental materials are available at http://jnmt.snmjournals.org). For PYP− participants, GLS correlated strongly with the apical, mid, and basal regions, with a Pearson correlation coefficient of more than 0.6 ($P < 0.001$). The apical region was significantly strongly associated with the mid region, with a correlation coefficient of 0.7 ($P < 0.001$), but was not significantly associated with the basal region, with a small correlation coefficient of 0.28 ($P = 0.08$) (Supplemental Tables 1 and 2). For PYP+, GLS correlated strongly with the apical and mid regions but not with the basal region, with a strong Pearson correlation coefficient of more than 0.8 ($P < 0.001$) for the apex and mid region but 0.22 ($P = 0.32$) for the basal region. The apical region was significantly associated with the mid region, with a medium Pearson correlation coefficient of 0.55 ($P = 0.009$), but not with the basal region ($P = 0.44$). The mid region was not significantly associated with the basal region ($P = 0.92$). The basal region was not statistically associated with the global, apical, or mid regions ($P > 0.05$ for all) (Supplemental Tables 3 and 4).

RESULTS

Patient Demographics and Variables

In total, 77 consecutive patients were identified, and 64 were included in the final analysis. The mean age of the participants was 75.1 ± 2.9 y, ranging from 41 to 103 y. PYP+ patients were significantly older than PYP− patients (81.0 ± 8.4 vs. 72.0 ± 13.8, $P = 0.002$). Male participants represented 89.1% of all participants, and there were no female participants in the PYP+ group; however, differences in the sex distributions between the 2 groups were not statistically significant. LV septal thickness (18.3 ± 3.0 vs. 14.1 ± 3.4 mm, $P = 0.0001$) and posterior wall thickness (16.4 ± 2.6 vs. 13.1 ± 3.0 mm, $P = 0.0004$), LV mass (352.3 ± 108.5 vs. 272.4 ± 101.5 g, $P = 0.005$), and LV mass index (175.7 ± 51.8 vs. 137.2 ± 42.5 g/m^2, $P = 0.002$) were significantly higher in the PYP+ group. There was no difference in mortality rate between the 2 groups. Patient demographics and selected variables with a breakdown per PYP group are outlined in Table 1.

Global and Regional Longitudinal Strain Comparison

The global, apical, mid, and basal regions were compared between participants with any ^{99m}Tc-PYP positivity and those with a completely negative scan (Table 2). The average GLS (PYP+ vs. PYP−, −10.5 ± 2.6 vs. −13.1 ± 4.1; $P = 0.003$) and the average basal segment longitudinal strain (−4.6 ± 2.6 vs. −8.8 ± 4.0, $P < 0.001$) differed significantly between the PYP+ and PYP− groups, with the PYP+ group having

TABLE 1
Patient Demographics

Demographic	PYP+ (n = 22)	PYP− (n = 42)	Total (n = 64)	P
Age	81.0 (8.4)	72.0 (13.8)	75.1 (12.9)	0.002*
Sex, male	22 (100.0%)	35 (83.3%)	57 (89.1%)	0.09†
Body mass index	27.0 (3.5)	27.2 (5.3)	27.1 (4.8)	0.89*
Systolic blood pressure (mm Hg)	119.8 (16.4)	136.6 (27.5)	130.6 (25.3)	0.029†
Diastolic blood pressure (mm Hg)	73.7 (11.93)	80.5 (15.73)	78.1 (14.74)	0.070†
Hypertension	12 (63.2%)	25 (73.5%)	37 (69.8%)	0.536†
History of coronary artery disease	6 (31.6%)	10 (29.4%)	16 (30.2%)	1.000†
History of diabetes mellitus	2 (10.5%)	10 (29.4%)	12 (22.6%)	0.174†
β-blocker	10 (52.6%)	22 (64.7%)	32 (60.4%)	0.559†
Calcium channel blocker	1 (5.3%)	9 (26.5%)	10 (18.9%)	0.076†
Angiotensin-converting-enzyme inhibitor	3 (15.8%)	5 (14.7%)	8 (15.1%)	1.000†
Angiotensin receptor blocker	5 (26.3%)	5 (14.7%)	10 (18.9%)	0.465†
Spironolactone	4 (21.1%)	5 (14.7%)	9 (17.0%)	0.706†
Amiodarone	0 (0.0%)	1 (2.9%)	1 (1.9%)	1.000†
Creatine	1.3 (1.1–1.5)	1.3 (1.1–1.8)	1.3 (1.1–1.7)	0.44‡
N-terminal prohormone B-type natriuretic protein	3,095.0 (1,640.0–7,323.0)	3,097.0 (1,238.5–8,832.5)	3,097.0 (1,407.0–7,447.0)	0.99‡
Low voltage on electrocardiography	6 (28.6%)	5 (11.9%)	11 (17.5%)	0.1575†
LV septal wall thickness (mm)	18.3 (2.96)	14.1 (3.43)	15.7 (3.83)	0.0001*
LV posterior wall thickness (mm)	16.4 (2.63)	13.1 (2.99)	14.3 (3.28)	0.0004*
LV mass (g)	352.3 (108.5)	272.4 (101.5)	300.7 (110.1)	0.005*
LV mass index (g/m^2)	175.7 (51.8)	137.2 (42.5)	150.4 (49.1)	0.002*
LV End-diastolic diameter (mm)	44.5 (6.69)	47.2 (6.95)	46.2 (6.91)	0.143*
Ejection fraction (%)	47.9 (15.2)	51.8 (15.2)	50.5 (15.2)	0.34*
Stroke volume (mL)	65.6 (25.7)	76.4 (25.1)	72.5 (25.6)	0.1146‡
Cardiac index (L/m^2/min)	2.4 (0.83)	2.8 (0.88)	2.6 (0.88)	0.075†
Tricuspid annular plane systolic excursion by M-mode (mm)	12.3 (3.30)	17.2 (5.36)	15.8 (5.29)	0.0250‡
Pericardial effusion	8 (36.4%)	6 (14.3%)	14 (21.9%)	0.0584†
Heart-to-contralateral ratio	1.7 (0.4)	1.1 (0.2)	1.3 (0.4)	<0.001†
PYP scale¶	0 (0.0%)	30 (71.4%)	30 (46.9%)	<0.001†
0	2 (9.1%)	7 (16.7%)	9 (14.1%)	
1	6 (27.3%)	2 (4.8%)	8 (12.5%)	
2	14 (63.6%)	3 (7.1%)	17 (26.6%)	
3	0 (0.0%)	30 (71.4%)	30 (46.9%)	

*Unequal-variance 2-sample t test.
†Fisher exact test.
‡Wilcoxon rank-sum test.
¶Qualitative value for interpretation is determined by comparing uptake in myocardium. Grade 0 = no myocardial uptake, grade 1 = myocardial uptake less than bone uptake, grade 2 = myocardial uptake equal to bone uptake, grade 3 = myocardial uptake greater than bone uptake.
Qualitative data are number and percentage; continuous data are mean and SD or median and interquartile range.

worse myocardial function. A trend was observed in the average midsegment longitudinal strain (-9.6 ± 4.0 vs. -11.7 ± 4.4, $P = 0.07$). In contrast, there was no statistical difference in the average apical longitudinal strain between the 2 groups (-17.6 ± 4.7 vs. -19.0 ± 6.5, $P = 0.35$). RALSI was found to be 1.3 ± 0.5 in PYP+ patients and 1.0 ± 0.3 in PYP− patients ($P = 0.008$). The global and regional longitudinal strain analysis, along with RALSI, demonstrated overall worse myocardial function in PYP+ patients, with an apex-sparing pattern.

TABLE 2
Regional Comparison in PYP+ Vs. PYP− Participants Using 17-Segment Model

Region	PYP + (n = 22)	PYP− (n = 42)	Total (n = 64)	P*
Global (%)	−10.5 (2.6)	−13.1 (4.1)	−12.2 (3.9)	0.003
Apex (%)	−17.6 (4.7)	−19.0 (6.5)	−18.5 (5.9)	0.35
Mid (%)	−9.6 (4.0)	−11.7 (4.4)	−11.0 (4.6)	0.07
Basal (%)	−4.6 (2.6)	−8.8 (4.0)	−7.3 (4.1)	<0.001

*2-sample t test.

Segment-to-Segment Comparison

Segment-to-segment analysis (Table 3) demonstrated a statistically significant difference in strain between PYP+ and PYP− patients in 4 segments: basal inferior ($P = 0.006$), basal anterolateral ($P = 0.01$), apical septal ($P = 0.002$), and apical inferior ($P = 0.001$). No other segments demonstrated a statistically significant difference. The segments with a significant difference in strain were in either the basal or the apical segments.

Comparison of LV Diastolic Dysfunction

LV diastolic dysfunction significantly differed between the 2 groups, occurring in 17 (77.3%) patients in the PYP+ group versus 15 (36.6%) in the PYP− group ($P = 0.002$). When the PYP+ group was compared with the PYP− group, the medial E/e′ ratio was significantly higher in the PYP+ group, and the mean mitral A wave velocity and the medial and lateral e′ velocity measurements were significantly lower in the PYP− group. Also, we observed trends toward a higher mean E/A ratio and lateral E/e′ ratio in the PYP+ group. These data consistently demonstrated worse diastolic function in PYP+ patients. Detailed data are summarized in Table 4.

DISCUSSION

Our CA patient cohort had a similar age, sex, and race distribution to that in published data (*10,21–23*); the absence of female cases in the PYP+ group was likely due to the small sample size, as PYP+ is known to have a male-predominant population according to previous reports. LV mass and LV mass index were significantly higher in PYP+ patients. PYP+ patients were older than PYP− patients. To the best of our knowledge, this was the first study that demonstrated a difference in global and regional strain patterns among the TTR subtype CA, as determined by ^{99m}Tc-PYP imaging, and provided a segment-to-segment comparison between PYP+ and PYP− segments. Our study showed the correlations

TABLE 3
Segment-to-Segment Comparison in PYP+ Vs. PYP− Participants Using 17-Segment Model Individually

		PYP−		PYP+		
Segment	Region	n	Mean (%)	n	Mean (%)	P*
Basal	Anterior	49	−8.5 (6.82)	12	−5.7 (4.31)	0.17
	Anteroseptal	54	−13.3 (7.58)	8	−14.3 (6.86)	0.73
	Inferoseptal	50	−19.3 (8.09)	9	−20.3 (7.55)	0.71
	Inferior	44	−8.7 (6.44)	16	−3.3 (6.27)	0.006
	Inferolateral	46	−11.7 (8.40)	15	−10.9 (6.51)	0.74
	Anterolateral	51	−19.7 (8.63)	9	−11.8 (8.57)	0.01
Mid	Anterior	45	−8.3 (6.00)	18	−6.3 (4.69)	0.20
	Anteroseptal	40	−10 (5.92)	21	−8.4 (4.63)	0.31
	Inferoseptal	41	−18.9 (8.91)	22	−18.0 (5.69)	0.61
	Inferior	45	−9.4 (8.64)	18	−7.6 (6.12)	0.42
	Inferolateral	48	−9.1 (6.12)	14	−7.9 (4.07)	0.52
	Anterolateral	49	−16.4 (8.25)	14	−15.6 (6.44)	0.76
Apical	Anterior	51	−12.4 (4.80)	12	−10.2 (3.09)	0.15
	Septal	41	−13.1 (4.96)	22	−9.9 (2.85)	0.002
	Inferior	42	−13.1 (4.90)	21	−9.7 (2.80)	0.001
	Lateral	51	−12.4 (4.76)	12	−10.2 (3.31)	0.13
	Apex	55	−12.2 (4.67)	8	−10.5 (3.83)	0.33

*2-sample t test.
Data in parentheses are SDs.

TABLE 4
LV Diastolic Function Parameters

Parameter	PYP+ (n = 22)	PYP− (n = 42)	Total (n = 64)	P
Presence of diastolic dysfunction	17 (77.3%)	15 (36.6%)	32 (50.0%)	0.002*
Peak tricuspid regurgitation velocity (m/s)	2.7 (0.44)	2.9 (0.46)	2.8 (0.46)	0.176†
Right ventricular systolic pressure (mm Hg)	40.3 (12.7)	44.1 (15.1)	42.8 (14.3)	0.3370‡
E-wave velocity (m/s)	0.9 (0.8–1.0)	0.8 (0.7–1.0)	0.9 (0.7–1.0)	0.70†
A-wave velocity (m/s)	0.5 (0.3–0.7)	0.8 (0.6–0.9)	0.7 (0.5–0.9)	0.03†
E/A ratio	2.0 (1.1–3.0)	1.2 (0.9–1.8)	1.3 (1.0–2.0)	0.06†
E deceleration time (ms)	154.5 (140.0–189.0)	178.0 (139.0–205.0)	170.0 (140.0–205.0)	0.46†
Tissue doppler medial e′ > velocity (cm/s)	3.3 (1.9)	4.7 (1.7)	4.2 (1.9)	0.009†
Tissue doppler lateral e′ > velocity (cm/s)	4.4 (2.0)	6.3 (2.3)	5.6 (2.4)	0.009†
E/e′ ratio medial	32.4 (18.3)	22.0 (12.1)	25.8 (15.3)	0.02‡
E/e′ ratio lateral	21.8 (9.2)	17.0 (10.3)	18.8 (10.1)	0.07‡

*Fisher exact test.
†Wilcoxon rank-sum test.
‡2-sample t test.
Qualitative data are number and percentage; continuous data are mean and SD or median and interquartile range.

between ^{99m}Tc-PYP uptake and myocardial strain function impairment and provided insight on the underlying mechanism.

Correlations Between ^{99m}Tc-PYP Uptake and Myocardial Strain Function Impairment

Our results demonstrated an overall compromised myocardial strain function and the basal-to-apex gradient (apex sparing) in both PYP+ and PYP− groups, as is consistent with prior studies and again supports the concept of apex sparing regardless of the background pathogenesis of CA (*10,11, 24,25*). Our study further provided a head-to-head comparison between the 2 groups and revealed significantly worse LV GLS and basal regional strain in the PYP+ group, with a trend toward a worse mid ventricular regional strain and a relatively spared apical regional strain. This result is also reflected by the significantly higher RALSI in the PYP+ group, indicating a larger gradient of longitudinal strain. In the segment-to-segment comparison, the PYP+ segments generally had worse segmental strain function, despite not reaching statistical significance in every segment.

Our findings provided qualitative evidence for the correlations between ^{99m}Tc-PYP uptake and impaired myocardial strain function in patients with suspected CA. A previous European study found that quantified ^{99m}Tc-hydroxymethylene diphosphonate uptake in patients with TTR-related CA had an apex-sparing pattern similar to that of strain echo imaging (*13*) and suggested a higher amyloid burden in the basal region as the underlying mechanism. Our study supports the concept and further provided a head-to-head comparison of the nuclear tracer uptake and strain function, as echocardiography was not performed in the other study.

We also attempted to compare our results with prior studies that assessed myocardial strain function in different subtypes of CA. However, because of a lack of endomyocardial biopsy results to confirm the certain subtype, it is difficult to directly compare our results with these studies. Our PYP+ group contained TTR-related CA; however, this population can still include wild-type TTR and hereditary TTR, which may present with a different LV strain function (*10*). Quarta et al. reported better LV GLS in patients with hereditary TTR (−15% ± 4%) than in those with wild-type TTR (−11% ± 3%) or AL-type TTR (−12% ± 4%) in 172 endomyocardial biopsy–confirmed patients (*10*). Our PYP+ group had a mean LV GLS similar to that of the wild-type TTR group. Compared with Quarta's report, our PYP+ patients were 5–6 y older and had a higher LV mass index and mildly impaired LV ejection fraction (*10*), which can represent more severe phenotypes of the disease and therefore can be related to worse LV GLS. Another study reported no difference in LV GLS among 3 major subtypes (AL, wild-type TTR, and hereditary TTR) of CA, with an impaired LV GLS strain at about −10% (*11*). Surprisingly, despite the worse LV GLS across all 3 groups, all LV ejection fractions were within the reference range in their study. The above studies show that patients with hereditary TTR might have a heterogeneous presentation concerning their LV GLS, potentially explaining our observation of worse LV GLS in the PYP+ group.

Longitudinal strain impairment is known to correlate with amyloid burden as measured by histopathology staining and late gadolinium enhancement on cardiac MR images (*11*). Our observation suggests that longitudinal strain impairment is also related to ^{99m}Tc-PYP uptake from the segmental to the global level. Although the exact mechanism of PYP uptake remains unclear, a potential mechanism such as microcalcification of myocardial tissue may play a role in the development of strain function impairment (*14*). This possibility is also supported by Gucht et al., who observed an apex-sparing pattern of ^{99m}Tc-hydroxymethylene diphosphonate uptake (*13*).

The value of investigational amyloid PET agents in clinical trials and the literature for diagnosis and investigation of CA has been encouraging. However, there is still a lack of convincing clinical evidence in distinguishing TTR CA from AL CA (*25*).

In brief, despite having a similar compromised GLS and basal-to-apex regional strain gradient pattern, the overall worse global strain function and higher RALSI can potentially be used to characterize PYP+ patients. With the advantage of being readily available and free of radiation, speckle-tracking strain imaging can become a more valuable noninvasive diagnostic tool in the assessment of CA by providing additional subtyping and prognostic information before an advanced imaging study such as ^{99m}Tc-PYP.

Diastolic Dysfunction in PYP+ or PYP− Patients

Although the apex-sparing strain pattern is characteristic in CA patients, diastolic dysfunction also plays an important role in their clinical presentation and can independently predict mortality (*26*). Diastolic dysfunction in CA patients has been observed in early studies and can deteriorate with progression of the disease (*27,28*). We observed significantly worse diastolic function measured by E/A ratio, medial and lateral e′ velocity, and E/e′ ratio in the PYP+ group than in the PYP− group. To the best of our knowledge, this was the first report to compare PYP+ and PYP− patients, and our findings indicate that ^{99m}Tc-PYP uptake can be a surrogate marker for worse cardiac diastolic function patients with suspected CA. Again, because the significantly older age in our PYP+ group may reflect a later stage of the disease, this result should be interpreted carefully.

Limitations

The study was limited by its retrospective, single-center design. The relatively low number of participants was due to the strict enrollment criteria for participants undergoing ^{99m}Tc-PYP scanning and, within 90 d, strain imaging at a single center. To sufficiently power future similar studies, participants will likely need to be enrolled from multiple centers. The comparison of strain imaging using the 18-segment model and ^{99m}Tc-PYP imaging using the 17-segment model was troublesome and may significantly compromise the segment-to-segment comparison of the apical strain. Efforts were made to minimize this discrepancy as much as possible. Because the intervals between ^{99m}Tc-PYP injection and scintigraphy scanning can lead to different false-positive rates among different protocols, caution should be take when generalizing our results to different scanning protocols.

With limited endomyocardial biopsy results, we were not able to further identify the patients in the PYP+ group as hereditary or wild-type TTR, which may present with different levels of myocardial strain dysfunction.

CONCLUSION

With the advance of imaging technology, noninvasive approaches such as ^{99m}Tc-PYP imaging have become an essential part in the diagnosis of CA, without the need for endomyocardial biopsy. Our study suggested that ^{99m}Tc-PYP uptake is related to overall worse LV segmental, regional, and GLS function, as well as diastolic function, than is no ^{99m}Tc-PYP uptake. Our work provides important data allowing clinicians to appreciate the echocardiographic features related to ^{99m}Tc-PYP uptake and can serve as a hypothesis-generating tool for future investigators.

DISCLOSURE

No potential conflict of interest relevant to this article was reported.

KEY POINTS

QUESTION: How do ^{99m}Tc-PYP imaging and echocardiographic strain imaging compare in the assessment of TTR CA?

PERTINENT FINDINGS: Our study suggested that ^{99m}Tc-PYP uptake is related to overall worse LV segmental, regional, and GLS function, as well as diastolic function, compared with no ^{99m}Tc-PYP uptake.

IMPLICATIONS FOR PATIENT CARE: These data are important for helping clinicians learn about the echocardiographic function features related to ^{99m}Tc-PYP uptake and can help generate hypotheses for future studies.

REFERENCES

1. Dubrey SW, Hawkins PN, Falk RH. Amyloid diseases of the heart: assessment, diagnosis, and referral. *Heart.* 2011;97:75–84.
2. Larsen BT, Mereuta OM, Dasari S, et al. Correlation of histomorphological pattern of cardiac amyloid deposition with amyloid type: a histological and proteomic analysis of 108 cases. *Histopathology.* 2016;68:648–656.
3. Maleszewski JJ. Cardiac amyloidosis: pathology, nomenclature, and typing. *Cardiovasc Pathol.* 2015;24:343–350.
4. Gertz MA, Comenzo R, Falk RH, et al. Definition of organ involvement and treatment response in immunoglobulin light chain amyloidosis (AL): a consensus opinion from the 10th international symposium on amyloid and amyloidosis. *Am J Hematol.* 2005;79:319–328.
5. Ruberg FL, Grogan M, Hanna M, Kelly JW, Maurer MS. Transthyretin amyloid cardiomyopathy. *J Am Coll Cardiol.* 2019;73:2872–2891.
6. Williams LK, Frenneaux MP, Steeds RP. Echocardiography in hypertrophic cardiomyopathy diagnosis, prognosis, and role in management. *Eur J Echocardiogr.* 2009;10:iii9–iii14.
7. Pagourelias ED, Mirea O, Duchenne J, et al. Echo parameters for differential diagnosis in cardiac amyloidosis. *Circ Cardiovasc Imaging.* 2017;10:e005588.
8. Phelan D, Collier P, Thavendiranathan P, et al. Relative apical sparing of longitudinal strain using two-dimensional speckle-tracking echocardiography is both sensitive and specific for the diagnosis of cardiac amyloidosis. *Heart.* 2012;98:1442–1448.
9. Liu D, Hu K, Nordbeck P, Ertl G, Störk S, Weidemann F. Longitudinal strain bull's eye plot patterns in patients with cardiomyopathy and concentric left ventricular hypertrophy. *Eur J Med Res.* 2016;21:21.
10. Quarta CC, Solomon SD, Uraizee I, et al. Left ventricular structure and function in transthyretin-related versus light-chain cardiac amyloidosis. *Circulation.* 2014;129:1840–1849.
11. Ternacle J, Bodez D, Guellich A, et al. Causes and consequences of longitudinal LV dysfunction assessed by 2D strain echocardiography in cardiac amyloidosis. *JACC Cardiovasc Imaging.* 2016;9:126–138.
12. Perugini E, Guidalotti PL, Salvi F, et al. Noninvasive etiologic diagnosis of cardiac amyloidosis using ^{99m}Tc-3,3-diphosphono-1,2-propanodicarboxylic acid scintigraphy. *J Am Coll Cardiol.* 2005;46:1076–1084.
13. Gucht AVD, Cottereau A-S, Abulizi M, et al. Apical sparing pattern of left ventricular myocardial ^{99m}Tc-HMDP uptake in patients with transthyretin cardiac amyloidosis. *J Nucl Cardiol.* 2017;25:2072–2079.
14. Stats MA, Stone JR. Varying levels of small microcalcifications and macrophages in ATTR and AL cardiac amyloidosis: implications for utilizing nuclear medicine studies to subtype amyloidosis. *Cardiovasc Pathol.* 2016;25:413–417.

15. Witteles RM, Liedtke M. AL amyloidosis for the cardiologist and oncologist: epidemiology, diagnosis, and management. *JACC CardioOncol.* 2019;1:117–130.
16. Nagueh SF, Smiseth OA, Appleton CP, et al. Recommendations for the evaluation of left ventricular diastolic function by echocardiography: an update from the American Society of Echocardiography and the European Association of Cardiovascular Imaging. *J Am Soc Echocardiogr.* 2016;29:277–314.
17. Lang RM, Badano LP, Mor-Avi V, et al. Recommendations for cardiac chamber quantification by echocardiography in adults: an update from the American Society of Echocardiography and the European Association of Cardiovascular Imaging. *J Am Soc Echocardiogr.* 2015;28:1–39.e14.
18. Cerqueira MD, Weissman NJ, Dilsizian V, et al.; American Heart Association Writing Group on Myocardial Segmentation and Registration for Cardiac Imaging. Standardized myocardial segmentation and nomenclature for tomographic imaging of the heart: a statement for healthcare professionals from the Cardiac Imaging Committee of the Council on Clinical Cardiology of the American Heart Association. *Circulation.* 2002;105:539–542.
19. Bokhari S, Castaño A, Pozniakoff T, Deslisle S, Latif F, Maurer MS. ^{99m}Tc-pyrophosphate scintigraphy for differentiating light-chain cardiac amyloidosis from the transthyretin-related familial and senile cardiac amyloidoses. *Circ Cardiovasc Imaging.* 2013;6:195–201.
20. Dorbala S, Ando Y, Bokhari S, et al. ASNC/AHA/ASE/EANM/HFSA/ISA/SCMR/SNMMI expert consensus recommendations for multimodality imaging in cardiac amyloidosis: part 1 of 2—evidence base and standardized methods of imaging. *J Nucl Cardiol.* 2019;26:2065–2123.
21. Sperry BW, Vranian MN, Hachamovitch R, et al. Subtype-specific interactions and prognosis in cardiac amyloidosis. *J Am Heart Assoc.* 2016;5:e002877.
22. Pinney JH, Whelan CJ, Petrie A, et al. Senile systemic amyloidosis: clinical features at presentation and outcome. *J Am Heart Assoc.* 2013;2:e000098.
23. Connors LH, Sam F, Skinner M, et al. Heart failure resulting from age-related cardiac amyloid disease associated with wild-type transthyretin. *Circulation.* 2016;133:282–290.
24. Nardozza M, Chiodi E, Mele D. Left ventricle relative apical sparing in cardiac amyloidosis. *J Cardiovasc Echogr.* 2017;27:141–142.
25. Yang M, Arsanjani R, Roarke MC. Advanced nuclear medicine and molecular imaging in the diagnosis of cardiomyopathy. *AJR.* 2020;215:1208–1217.
26. Chacko L, Martone R, Bandera F, et al. Echocardiographic phenotype and prognosis in transthyretin cardiac amyloidosis. *Eur Heart J.* 2020;41:1439–1447.
27. Hartmann A, Frenkel J, Hopf R, et al. Is technetium-99m-pyrophosphate scintigraphy valuable in the diagnosis of cardiac amyloidosis? *Int J Card Imaging.* 1990;5:227–231.
28. Klein AL, Hatle LK, Burstow DJ, et al. Doppler characterization of left ventricular diastolic function in cardiac amyloidosis. *J Am Coll Cardiol.* 1989;13:1017–1026.